JACS
JOURNAL OF THE AMERICAN CHEMICAL SOCIETY

Article

pubs.acs.org/JACS

# Diffusion-Limited Cargo Loading of an Engineered Protein Container

Reinhard Zschoche and Donald Hilvert*

Laboratory of Organic Chemistry, ETH Zürich, 8093 Zürich, Switzerland

Supporting Information

**ABSTRACT:** The engineered bacterial nanocompartment AaLS-13 is a promising artificial encapsulation system that exploits electrostatic interactions for cargo loading. In order to study its ability to take up and retain guests, a pair of fluorescent proteins was developed which allows spectroscopic determination of the extent of encapsulation by Förster resonance energy transfer (FRET). The encapsulation process is generally complete within a second, suggesting low energetic barriers for proteins to cross the capsid shell. Formation of intermediate aggregates upon mixing host and guest in vitro complicates capsid loading at low ionic strength, but can be sidestepped by increasing salt concentrations or diluting the components. Encapsulation of guests is completely reversible, and the position of the equilibrium is easily tuned by varying the ionic strength. These results, which challenge the notion that AaLS-13 is a continuous rigid shell, provide valuable information about cargo loading that will guide ongoing efforts to engineer functional host−guest complexes. Moreover, it should be possible to adapt the protein FRET pair described in this report to characterize functional capsid−cargo complexes generated by other encapsulation systems.

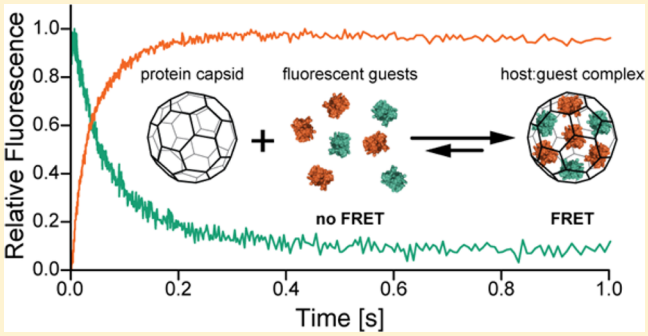


## INTRODUCTION

Icosahedral capsids are a striking example of nature's extraordinary ability to self-organize on a molecular level. Over the last few decades, research on their most prominent representatives, the shells that constitute the protective coats of viruses, has revealed the importance of precisely tuned interactions between individual subunits. The sensitivity of these attractive forces to pH, ionic strength, and temperature ensures that formation of kinetically trapped off-pathway aggregates is minimized and assembly occurs only in response to a specific stimulus at the end of the infectious cycle.[1−4] Once formed, viral shells are remarkably resistant to a broad spectrum of environmental conditions and often disintegrate only upon encountering a suitable host. This resilience, together with the ability of some capsids to assemble even in the absence of their native nucleic acids, has sparked considerable interest in applying virus-like particles in materials science, biotechnology, and medicine.[5−7] Their repetitive and symmetric structures provide an ideal scaffold for spatially defined modifications that transform them into multivalent binders[8] and building blocks for ordered nanomaterials.[9] The ability to confine a wide range of cargo molecules and release them in response to a variety of triggers makes viral capsids attractive candidates for targeted delivery of drugs[10] and contrast agents[11] or as nanoreactors for chemical and biochemical reactions.[12,13]

Symmetric polyhedral architecture is not unique to viral shells, but also a feature of bacterial microcompartments (BMCs).[14−16] Despite their morphological similarity, evolutionary pressures disparate from those for viruses might have led to a different set of structural and dynamic properties.[17] BMCs are considered a poor cell's substitute for membrane-enclosed subcellular spaces, allowing prokaryotes to coordinate metabolic pathways that produce cytotoxic intermediates or channel metabolites between enzymes. In contrast to viral capsids, they must therefore allow passage of small molecules.[14,17,18] Since they can be easily produced and self-assembled in bacterial cells, BMC-derived protein shells are amenable to directed evolution experiments[19] and thus of particular interest as artificial encapsulation systems.[20] This strategy is promising not only for understanding BMC function and any associated evolutionary advantages but also for engineering building blocks for synthetic biology that have the potential to expand the biotechnological utility of prokaryotes by enhancing pathway fluxes or installing completely new pathways.[21,22]

Viral capsids and BMCs alike have been loaded with diverse cargo using covalent peptide linkers,[23] as well as a variety of supramolecular interactions including coiled-coils,[24] RNA aptamers,[25] peptide-binding motifs,[26] and electrostatic attraction.[27−29] In view of the high stability of viral capsids,[30] the resulting capsid−cargo complexes are presumed to be stable, as convincingly demonstrated for bacteriophage P22, which retains cargo proteins even after selective proteolytic removal of a scaffolding protein.[23]

For tethering systems based on reversible interactions, it is possible that encapsulated cargo molecules are in equilibrium with free cargo, provided they can traverse the capsid shells.

**Received:** October 9, 2015
**Published:** December 4, 2015





DOI: 10.1021/jacs.5b10588
J. Am. Chem. Soc. 2015, 137, 16121−16132

However, structures of viral capsids and bacterial microcompartments generally show closed polyhedral structures with small if any pores. The high kinetic barriers for dissociation of subunits from protein shells[31] further suggest that escape of cargo, once encapsulated, should be physically difficult. Nevertheless, the substantial modifications that are sometimes introduced to engineer capsids for particular applications might considerably alter the structure and stability of the resulting constructs. Moreover, proteinaceous bacterial compartments might be significantly more flexible than viral capsids as they require a constant influx and efflux of metabolites to function. For example, riboflavin synthase is encapsulated by the enzyme lumazine synthase, which assembles as a 60-subunit dodecahedron.[32] Since the pores found in the crystal structures of lumazine synthases are not large enough to allow passage of riboflavin,[33] the capsid would have to temporarily adopt a significantly altered conformation to allow exit of the product.

Our laboratory has engineered the lumazine synthase from the thermophilic bacterium *Aquifex aeolicus* (AaLS) to encapsulate positively charged cargo molecules. Four glutamates were introduced on the lumenal face of each monomer to give the variant AaLS-neg, which encapsulates GFP molecules possessing a deca-arginine tag.[27] The capsid's ability to retain proteins tagged with a positively charged peptide was subsequently improved by directed evolution.[34] The resulting variant, AaLS-13, has a total of 11 mutations and forms capsids with an increased diameter (35.4 ± 3.2 nm compared to 28.6 ± 2.6 nm for AaLS-neg and 15.4 nm for wild-type AaLS).[34,35] It can be noncovalently loaded with positively charged cargo proteins in vivo and in vitro.[29,34] For example, mixing positively supercharged green fluorescent protein (GFP36+)[36] with capsid fragments affords capsids filled with cargo. Identical guest–capsid complexes are obtained upon mixing guests with already assembled capsids (Figure 1). AaLS-13 capsids are even able to incorporate particles as large as ferritin ($d$ = 12 nm),[37] suggesting either an atypical uptake mechanism or partial reversibility of capsid assembly. While the encapsulation of cargo concurrent with capsid formation from fragments is intuitive, the entry of large cargo proteins into assembled capsids is surprising and to our knowledge without precedent.

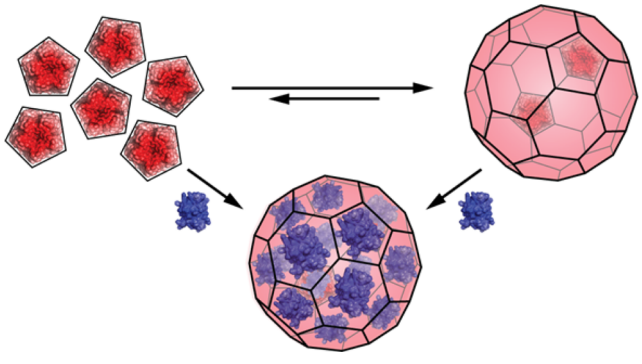

**Figure 1.** AaLS-13 encapsulation system. Rational design and directed evolution endowed the lumenal face of the AaLS capsid with substantial negative charge (red). Capsid fragments (largely pentamers) spontaneously assemble to capsids in vitro in the presence of positively supercharged GFP36+ (blue) affording cage complexes. Analogous complexes are obtained upon mixing GFP36+ with assembled AaLS-13 capsids.[29] Since the structure of assembled AaLS-13 is unknown, a hypothetical truncated icosahedron is used to depict the capsid.

Since the microscopic and macroscopic stabilities of capsid–cargo complexes are decisive parameters for biotechnological applications, we developed a positively supercharged protein pair that allows spectroscopic investigation of the extent of encapsulation by changes in Förster resonance energy transfer efficiency (FRET), a phenomenon that has been exploited to characterize other engineered guest–capsid systems.[38,39] By virtue of this technique we gained unprecedented insight into the kinetics of the encapsulation process and the stability of the capsid–cargo complexes. This methodology can be adapted to other encapsulation strategies and will be a useful tool to evaluate the suitability of individual capsids and tethers for the construction of drug delivery vehicles or artificial organelles.

## RESULTS

**A Protein FRET Pair.** Introducing four mutations, T65G, S72A, K79R and T203Y (numbering with respect to wild-type GFP), into GFP36+[36] afforded TOP36+, named after Topaz, a yellow fluorescent protein (YFP) obtained by introducing the same mutations into wild-type GFP.[40] The absorption maximum of TOP36+ is red-shifted to 513 nm ($\varepsilon$ = 69,800 $M^{-1}$ $cm^{-1}$) versus 488 nm ($\varepsilon$ = 36,600 $M^{-1}$ $cm^{-1}$) for GFP36+. Analogously, whereas GFP36+ displays maximum emission at 508 nm, the emission maximum of TOP36+ is red-shifted to 525 nm. The quantum yield is similar for both variants (0.52 ± 0.03 for GFP36+ and 0.55 ± 0.03 for TOP36+) and independent of the excitation wavelength between 410 and 450 nm.

Encapsulation of GFP36+ by AaLS-13 capsids[29] has only a marginal effect (2%) on its fluorescence. In contrast, the fluorescence of TOP36+ is increased up to 10% upon internalization (Figure S1). It is well-known that chloride ions decrease the fluorescence of YFPs.[41] The enhanced fluorescence upon encapsulation is thus likely attributable to a lowered affinity for chloride, which is present in the standard assay buffer (50 mM $NaP_i$, 200 mM NaCl, 5 mM EDTA, pH 8.0, $I$ = 350 mM), owing to the more negative electric potential within the AaLS-13 capsid.

GFP and YFP have the longest Förster distance and hence the highest FRET efficiency of characterized fluorescent protein pairs.[42] Overlaying the emission and excitation spectra of GFP36+ and TOP36+ reveals that this property is preserved after supercharging (Figure 2A). The emission peak of GFP36+ overlaps with the excitation peak of TOP36+, and while TOP36+ shows little absorption at 400 nm, GFP36+ is still considerably excited. Addition of purified AaLS-13 capsids to a mixture of the two fluorescent proteins increases the emission maximum from 508 to 525 nm upon selective excitation of GFP36+, indicating that co-confinement of the two fluorescent proteins in the AaLS-13 capsid decreases their average distance to close to the Förster distance of around 5 Å[42] and thus drastically enhances FRET efficiency (Figure 2B). The most pronounced change is observed for a GFP36+:TOP36+ ratio of 1:4, in accord with the finding that energy-transfer efficiency increases upon increasing the number of acceptors per donor.[43]

Although the precise assembly state of the AaLS-13 capsid has not been determined, the capsid diameter observed by negative-staining transmission electron microscopy (TEM) is consistent with symmetric polyhedral capsids having triangulation number $T$ = 3 or 4, corresponding to 180 or 240 subunits, respectively.[34] In the absence of detailed structural information and for the sake of simplicity, we report capsid loading assuming a 180-meric capsid structure.[29] Titrating


DOI: 10.1021/jacs.5b10588
J. Am. Chem. Soc. 2015, 137, 16121–16132

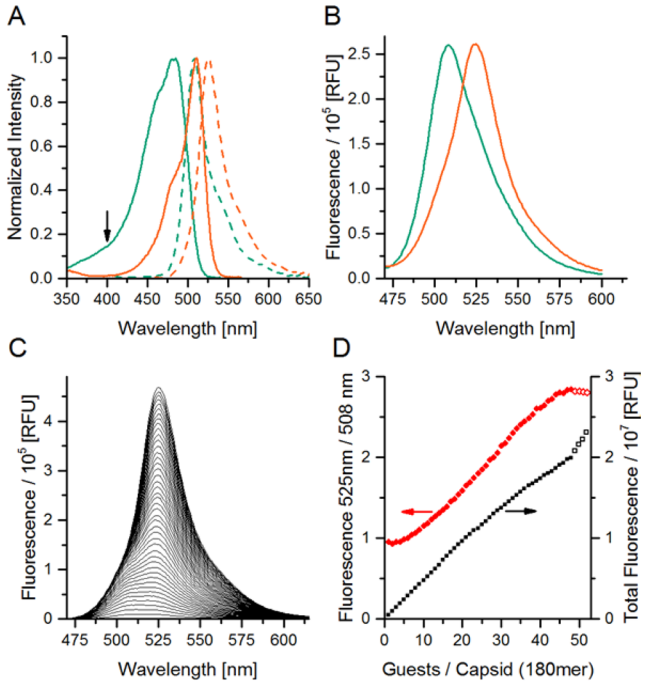


**Figure 2.** Fluorescence spectra of the GFP36+/TOP36+ FRET pair. (A) Normalized excitation (solid lines) and emission (dashed lines) spectra of GFP36+ (green) and TOP36+ (orange). The arrow indicates the wavelength at which GFP36+ can be selectively excitated. (B) Emission spectrum of a 1:4 GFP36+:TOP36+ mixture before (green) and after (orange) encapsulation in AaLS-13 capsids. (C) Emission spectra upon titrating 1−42 equiv of guest into an AaLS-13 capsid (180-mer). After addition of each equivalent, a fluorescence spectrum was recorded. (D) Ratio of emission at 525 and 508 nm (red diamonds) and total fluorescence (black squares) as a function of guest loading before (filled symbols) and after (open symbols) onset of aggregation.

AaLS-13 capsids with a 1:4 mixture of GFP36+ and TOP36+ demonstrates that the extent of FRET depends on capsid occupancy (Figure 2C). Between 10 and 46 guests per 180-mer, the relative emission at 525 nm/508 nm is linearly dependent on the number of guests per capsid and thus a suitable indicator for the extent of guest encapsulation (Figure 2D). At very low loading, donors and acceptors are far apart, whereas at high loading additional effects such as self-quenching become more prominent, resulting in decreased total fluorescence emission per guest. Exceeding the loading capacity (45 ± 2 guests per 180-mer capsid) leads to aggregation as judged by a sharp increase in light scattering. A decline in overall FRET efficiency and an increased total fluorescence per guest (Figure 2D, open symbols) suggest that the additional guests are not encapsulated.

Since FRET efficiency correlates with capsid occupancy, we attempted to leverage its distance dependency to estimate the number of subunits in the AaLS-13 capsid. While accurate determination of intermolecular distances from FRET between two fluorophores with well separated absorption and emission peaks is fairly straightforward,[44] such an analysis is semi-quantitative at best in the case of multiple encapsulated protein fluorophores. Assuming FRET between one donor and multiple acceptors that are uniformly distributed on a sphere, the data suggest that AaLS-13 capsids contain at least 240 subunits (Figure S9; see Supporting Information for a detailed description of the analysis). The exact composition will have to

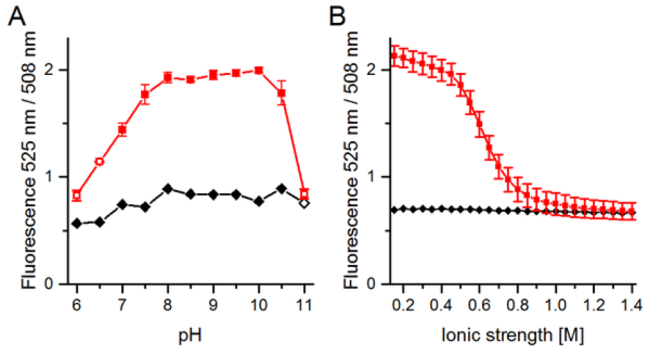


**Figure 3.** Relative fluorescence at 525 and 508 nm for a mixture of GFP36+/TOP36+ free in solution (black diamonds) or encapsulated by AaLS-13 (red squares) as a function of (A) pH and (B) ionic strength. Open symbols denote capsid precipitation (pH ≤ 6.5) or partial fluorophore degradation (pH ≥ 11.0). Error bars indicate the standard deviation from three independently prepared capsid−cargo complexes with 35 ± 3 guests per 180-mer capsid and a TOP36+:GFP36+ ratio of 4.0 ± 0.7.

be determined by cryo-electron microscopy or native mass spectrometry, which are routinely employed to characterize capsid structures.[45,46]

**Equilibrium Properties of Capsid−Guest Complexes.** A concentrated sample of AaLS-13 capsids containing a mixture of GFP36+ and TOP36+ was diluted in buffers of different pH, and the emission spectra were measured (Figure 3A). Between pH 8.0 and 10.0, the ratio of emission at 525 and 508 nm remains constant, indicating a stable guest−host complex. The decrease in FRET observed between pH 10−11 most likely reflects reduced affinity of the guest proteins to the capsid due to deprotonation of lysines in the positively supercharged guest proteins. Above pH 11.0 the fluorophores are slowly degraded. The decrease in FRET below pH 8.0 is more likely attributable to reduced fluorescence of TOP36+ relative to GFP36+ than guest release from the capsid, since the increased chromophore p$K_a$ of 6.6 for YFP versus 5.8 for GFP at 200 mM chloride is likely mirrored in the supercharged variants (Figure S1).[41]

Titrating concentrated aqueous NaCl into a solution of AaLS-13 capsids filled with a 1:4 mixture of GFP36+ and TOP36+ results in a decrease in TOP36+ emission and an increase in GFP36+ emission, reflecting decreasing FRET efficiency (Figure 3B). In order to exclude halide-dependent fluorescence quenching as the source of the decrease, the titration experiment was repeated with $Na_2SO_4$, which gave analogous results (Figure S4). Ionic strength-dependent release of guest proteins from capsids was confirmed by size-exclusion chromatography between $I$ = 150 and 1150 mM (Figure S2). TEM of the capsid-containing fractions shows exclusively intact capsids (Figure S3), demonstrating that AaLS-13 releases guest proteins without permanently compromising capsid integrity.

In order to determine whether cargo molecules are released from AaLS-13 capsids even at low ionic strength, capsids filled with GFP36+ and capsids filled with TOP36+ were mixed, and the change in fluorescence emission recorded (Figure 4A). Both the increase in emission at 525 nm and decrease at 508 nm follow an exponential time dependence, indicating rapid scrambling of cargo proteins between capsids. The half-life of this process is 37 ± 4 s for 32 guests/180-mer capsid at an ionic strength of 350 mM.

Exchange of guests could occur by three distinct mechanisms: (i) guests are transferred upon collision of at least two


DOI: 10.1021/jacs.5b10588
J. Am. Chem. Soc. 2015, 137, 16121−16132

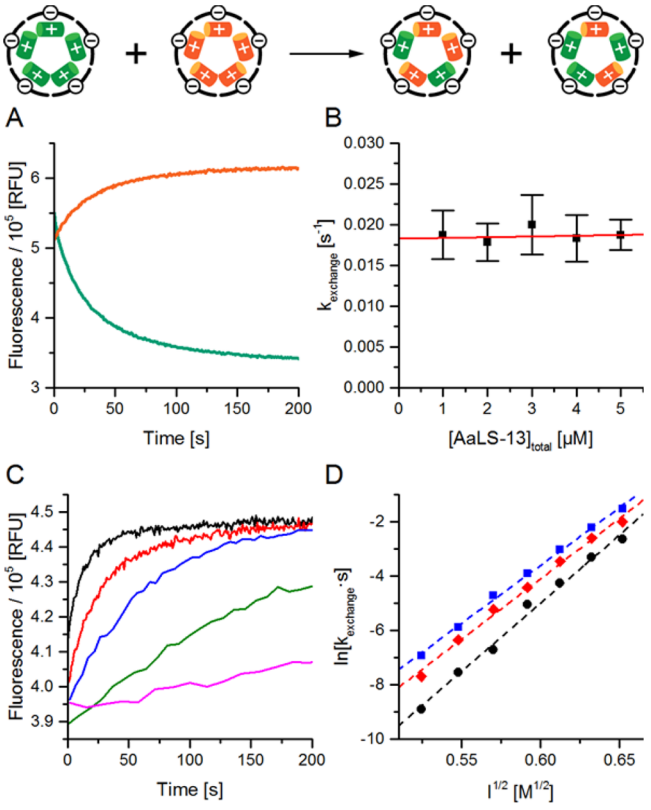


**Figure 4.** Guest exchange between filled AaLS-13 capsids. (A) Time-dependent emission at 508 nm (green) and 525 nm (orange) upon mixing capsids containing GFP36+ with capsids containing TOP36+ (32 guests/180-mer capsid, $I$ = 350 mM). (B) Rate of guest exchange as a function of capsid concentration (32 guests/capsid, $I$ = 350 mM). To a significance level <0.05, the exchange is not dependent on AaLS-13 concentration. (C) Traces of 525 nm emission for guest exchange between AaLS-13 capsids containing 22 guests/capsid at ionic strengths 425 mM (black), 400 mM (red), 375 mM (blue), 350 mM (green), and 325 mM (magenta). (D) Rate of guest exchange as a function of the square root of ionic strength for AaLS-13 capsids containing 22 guests/capsid (black circles), 28 guests/capsid (red diamonds), and 32 guests/capsid (blue squares).

capsids; (ii) guest molecules dissociate from one capsid and enter another; or (iii) capsid fragments with bound cargo detach and invade another capsid shell.

Figure 4B demonstrates that the rate of guest exchange is independent of capsid concentration, which excludes mechanisms in which the rate-determining step involves more than one capsid. Dissociation of a capsid subunit and subsequent incorporation into another capsid also appears unlikely based on an experiment in which empty capsids were covalently labeled with a fluorescent dye (Figures S5 and S6). No FRET was observed within 24 h of mixing AaLS-13 capsids labeled with ATTO-495 and capsids labeled with ATTO-565 (a FRET pair). A capsid assembled from fragments that were respectively labeled with the two fluorophores served as a positive control.

Having excluded both a bimolecular mechanism and the exchange of capsid fragments, transient dissociation of guest molecules from the capsid is the most likely explanation for guest exchange. The logarithm of the rate of exchange is linearly dependent on the square root of the ionic strength (Figure 4C,D), and the corresponding free energy of activation follows the same dependency. Since the free energy for Coulombic interactions in aqueous salt solutions scales with the

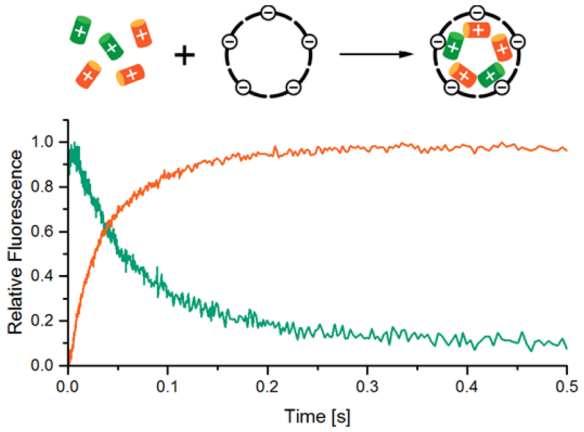


**Figure 5.** Fluorescence emission at 500 ± 5 nm (green) and >515 nm (orange) after mixing 20 $\mu$M empty AaLS-13 capsids with 4 $\mu$M 1:4 GFP36+/TOP36+ at $I$ = 550 mM in a stopped flow apparatus.

square root of ionic strength,[47,48] overcoming the electrostatic attraction between positively charged guest proteins and the negatively charged capsid shell is likely the rate-determining step. With increasing occupancy, the electrostatic binding energy per guest decreases as the attraction between the guest and the lumenal capsid surface is partially offset by electrostatic repulsion between guests, resulting in a faster guest exchange rate for more packed capsids (Figure 4D). This effect becomes less pronounced at higher ionic strength, which shields the charges on the protein surfaces more effectively.

**Kinetics of Guest Encapsulation.** Since the release of guest molecules from AaLS-13 capsids is clearly dominated by the strength of Coulombic interactions, we became interested in the rate of encapsulation. Previously, mixtures of GFP36+ and AaLS-13 capsids were incubated overnight before analysis by size-exclusion chromatography because we had assumed that loading would be slow.[29] However, preliminary kinetic experiments showed that the fluorescence changes attributed to co-encapsulation of GFP36+ and TOP36+ were already complete within a few seconds. We therefore monitored cargo loading by stopped-flow spectroscopy.

Guest molecules (GFP36+ and TOP36+ in a 1:4 ratio) and empty AaLS-13 capsids were mixed in a stopped-flow device at an ionic strength of 550 mM and fluorescence upon selective excitation of GFP36+ at 400 nm was followed. The time course of GFP36+ fluorescence was recorded using a band-pass filter with transmission between 495 and 505 nm; TOP36+ fluorescence was recorded using a long pass filter with transmission above 515 nm. Consistent with results presented in Figure 2, encapsulation increases FRET efficiency, as apparent from a decrease in GFP36+ donor emission and an increase in TOP36+ acceptor emission (Figure 5). To our surprise, however, encapsulation, as indicated by intermolecular FRET between guest molecules, was complete within 400 ms. Given the rigidity generally attributed to capsid shells[4,30] and failure to observe exchange of subunits between AaLS-13 capsids (Figure S6), rapid uptake of proteins as large as 30 kDa is startling. Consequently, several control experiments were performed to exclude spectroscopic artifacts.

When supercharged guest molecules were mixed with AaLS-13 capsids on a preparative scale, the solutions became instantly turbid but clarified within seconds. Turbidity is a result of an interaction between light and particles with diameters similar to the wavelength of the observed light. It can be detected


DOI: 10.1021/jacs.5b10588
J. Am. Chem. Soc. 2015, 137, 16121−16132

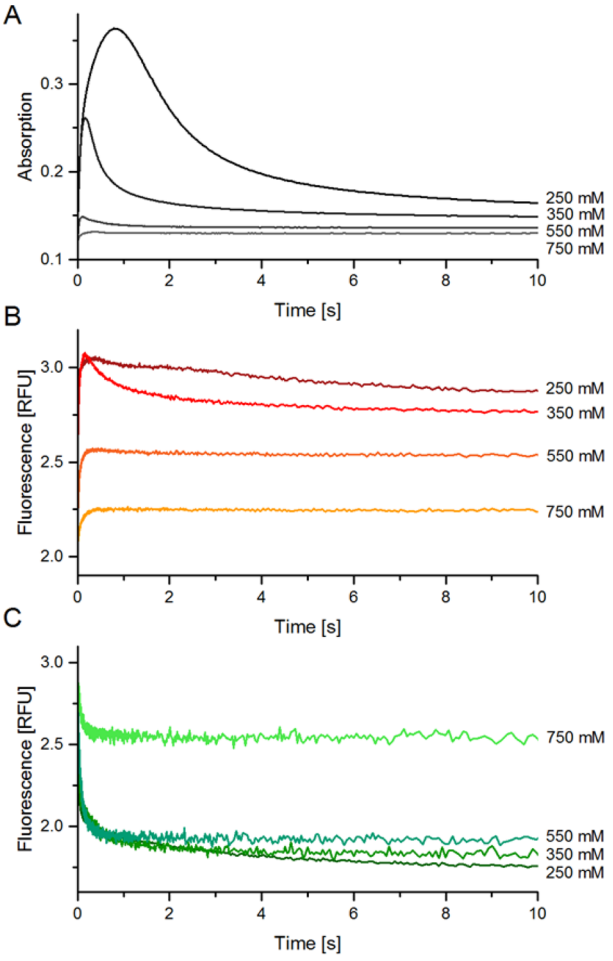


**Figure 6.** Progress curves after mixing 20 $\mu$M AaLS-13 capsids with 4 $\mu$M guest at different ionic strengths. Protein concentrations and instrument parameters were kept constant, allowing quantitative comparison. (A) Light scattering measured by absorption at 400 nm. (B) Emission >515 nm. (C) Emission 500 ± 5 nm.

spectroscopically by an increase in absorption proportional to $\lambda^{-4}$ or by light scattering quantified by a photomultiplier positioned at a 90° angle relative to the incident beam. Both techniques were employed in the stopped-flow setup to monitor the transient formation of the strongly scattering species generated upon mixing guests with capsids (Figure 6A).

The ionic strength at which guests and capsids are mixed has a profound impact on the progress curves observed by stopped flow spectroscopy (Figure 6). The decreasing amplitudes for changes in TOP36+ and GFP36+ emission upon increasing ionic strength reflect the reduced degree of encapsulation at higher salt concentrations. At low ionic strength ($I$ = 250 mM), an immediate and pronounced increase in light scattering is observed which relaxes within a few seconds. Simultaneously, the TOP36+ emission reaches a local maximum within a few hundred milliseconds and subsequently relaxes (Figure 6B). In contrast, GFP36+ emission decreases continuously in biphasic fashion (Figure 6C). The multiphasic fluorescence change traces, and the transient increase in light scattering indicate the existence of at least one intermediate during encapsulation.

This intermediate likely involves supercharged guests binding to the capsid exterior. Calculations of the surface electric potential of an AaLS-13 pentamer revealed a substantial negative charge on the outer surface (Figure 7). Using the

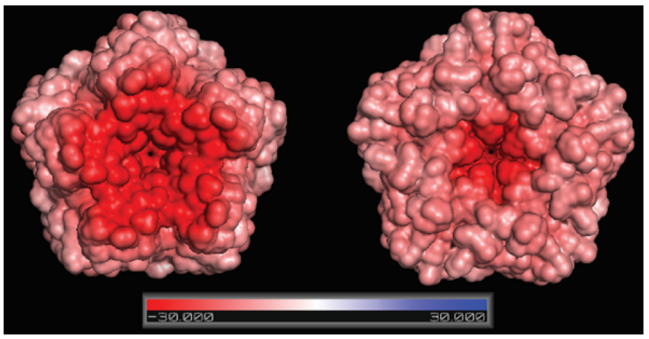


**Figure 7.** Electrostatic surface potential of the interior (left) and exterior surface (right) of a AaLS-13 pentamer at $I$ = 150 mM. The color gradient depicts the potential within ±30 $k_BT$/e.

APBS software,[49] the potential on the exterior face of the pentamer was calculated to be about two-thirds that of the interior face (−14 $k_BT$/e and −24 $k_BT$/e, respectively, at $I$ = 150 mM). Upon first encountering empty capsids, the positively charged guest molecules would initially bind to the negatively charged capsid exterior. Crossing the capsid shell and entering the lumen should then be limited, at least partially, by dissociation from the surface. In order to detach, the guests need to overcome the electrostatic attraction to the outer capsid wall, the strength of which is strongly dependent on the concentration of screening ions. In accordance with this hypothesis, the signals attributed to the aggregate—TOP36+ fluorescence and light scattering—are much less pronounced at higher ionic strength (Figure 6), indicating faster decay of the intermediate.

Whereas decay of the intermediate is likely a unimolecular process, its formation must be at least bimolecular and should therefore be concentration dependent. Indeed, when AaLS-13 capsids of different concentration are mixed with guests at a constant stoichiometric ratio, the signals associated with the intermediate become less intense with decreasing concentration, until below 7 $\mu$M AaLS-13 both signals show a continuous approach to equilibrium rather than a transient maximum (Figure 8A). Quantitative analysis of these progress curves is tempting but has to be undertaken with caution. Due to low FRET efficiency at low loading densities and

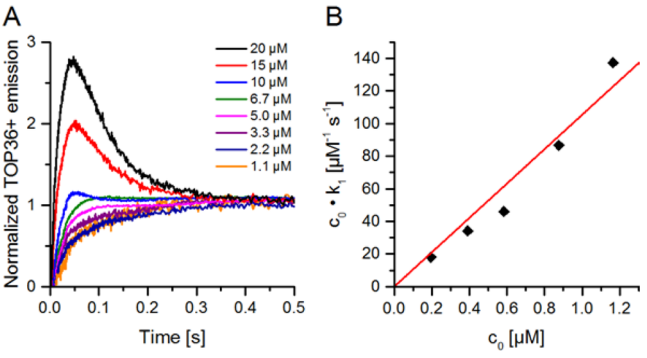


**Figure 8.** Concentration-dependent guest encapsulation by AaLS-13 capsids. (A) Progress curves for TOP36+ emission upon mixing 1:4 mixtures of GFP36+/TOP36+ with AaLS-13 at different protein concentrations (concentrations in legend with respect to AaLS-13 monomer). (B) Apparent rate constant for guest encapsulation as a function of initial protein concentration at an ionic strength of 350 mM.


DOI: 10.1021/jacs.5b10588
J. Am. Chem. Soc. 2015, 137, 16121−16132

precipitation induced by excess guest, only a narrow range of capsid:guest ratios can be probed, precluding experiments under pseudo-first-order conditions. Since pseudo-first-order experiments are impractical, association rates were estimated assuming second-order reactions between guests and capsids and fitting the progress curve to the corresponding rate law. Regression of the apparent rate constant against the initial concentrations of guests and binding sites within the capsids gave a bimolecular rate constant for encapsulation of GFP36+/TOP36+ mixtures of $10^8$ $M^{-1}$ $s^{-1}$ at 350 mM ionic strength, pH 8.0, 25 °C (Figure 8B). From the values of $k_{on}$ and $k_{off}$, the dissociation constant for the GFP36+/capsid complex is estimated to be about 0.2 nM. The effect of salt concentration on binding affinity can be approximated by the dependence of the rate constant for guest exchange on ionic strength (Figure 4D), assuming that $k_{on}$ is not significantly affected. The predicted stabilities agree well with the values observed by FRET (Figure S7).

**Probing the Encapsulation Mechanism with Fluorescently Labeled AaLS-13 Variants.** Existence of an intermediary complex with surface-bound guests rationalizes the transient increase in TOP36+ fluorescence, which is likely more environmentally sensitive than GFP36+, assuming that the trend observed for nonsupercharged GFP variants holds.[41,50] In order to obtain further evidence regarding the nature of this intermediate, we designed two capsid variants that were labeled with the FRET acceptor ATTO-565 on either the interior or exterior face of the capsid shell. If the intermediate has supercharged guests bound to the capsid exterior, FRET between TOP36+ and the fluorophore on the outer capsid surface should decrease simultaneously with the decay of this intermediate. The opposite trend should apply for capsids labeled on the lumenal face.

Since AaLS-13 contains three nucleophilic thiols per monomer, we created a variant named AaLS-RR (AaLS-13 C52R/C127R) by reverting two surface-exposed cysteine residues that had appeared during directed evolution to arginine as found in wild-type AaLS. The third thiol, Cys37, is buried, and its reactivity toward electrophilic labeling reagents is therefore expected to be negligible, particularly when substoichiometric amounts of fluorophore reagent are employed. Introduction of exposed cysteines into this variant afforded capsids that can be selectively labeled with ATTO-565-maleimide on either the interior (A85C) or exterior (R108C) surface.[51]

AaLS-RR is less negatively charged than AaLS-13 (because of re-introduction of two cationic arginines) and forms slightly smaller capsids with an average outer diameter of 32 ± 2 nm. In contrast to AaLS-13, capsid formation is reversible at an ionic strength of 350 mM. When purified AaLS-RR capsids are analyzed by size-exclusion chromatography, an approximately 1:1 mass ratio of assembled capsid to capsid fragments is obtained. Nevertheless, the changes in fluorescence upon encapsulation are qualitatively similar to those observed with AaLS-13 (Figure 9A). The lifetime of the transient intermediate is approximately 3-fold reduced compared to AaLS-13, presumably due to weaker Coulombic interactions between TOP36+ and the less charged AaLS-RR capsid. The most notable difference is the increase in both light scattering and TOP36+ fluorescence after 0.2 s, which was not observed for AaLS-13 (Figure 6), and probably reflects capsid formation from free capsid fragments triggered by binding of supercharged guest proteins. Although the AaLS-13 and AaLS-RR capsids are less alike than expected, the similar spectroscopic trends observed (Figures 7 and 9A) suggest that both capsid variants have analogous loading mechanisms.

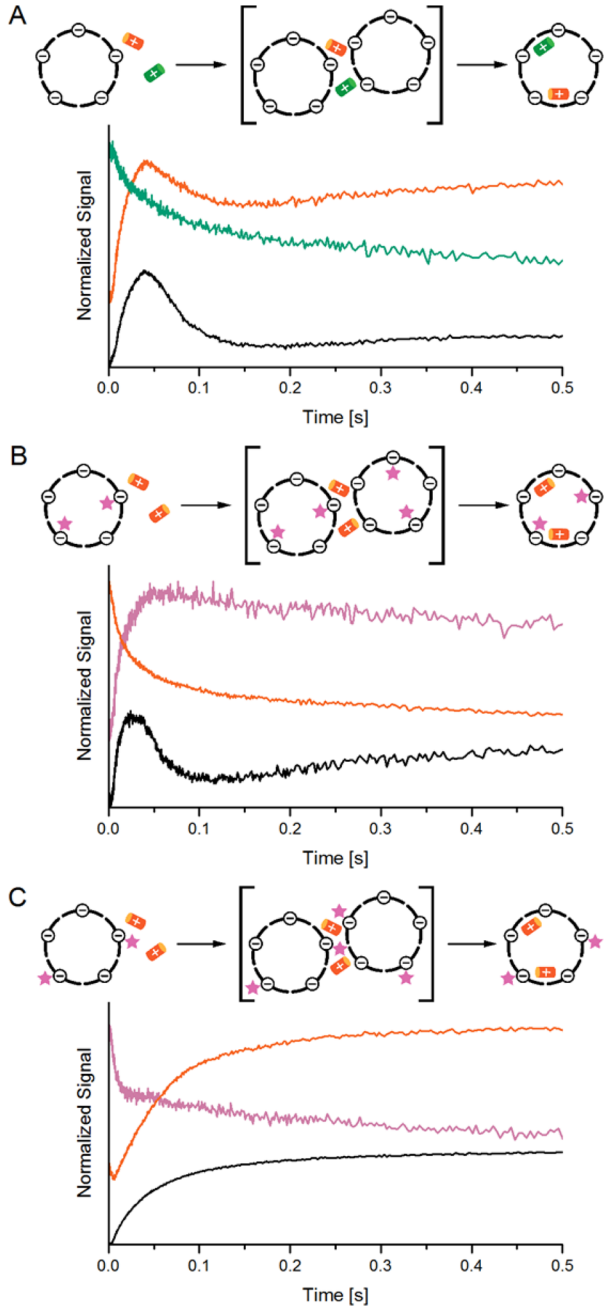


**Figure 9.** Change in GFP36+ emission (green), TOP36+ emission (orange), ATTO-565 emission (pink), and light scattering (black) after mixing 20 $\mu$M AaLS-RR variants with 4 $\mu$M guest proteins at $I$ = 350 mM. (A) Encapsulation of a GFP36+/TOP36+ 1:4 mixture into AaLS-RR. (B) Encapsulation of TOP36+ into AaLS-RR*$^{IN}$ labeled on the lumenal face. (C) Encapsulation of TOP36+ into AaLS-RR*$^{OUT}$ labeled on the exterior face.

The time course of the fluorescent signals observed upon mixing covalently labeled AaLS-RR capsids with TOP36+ indicates an initial interaction between TOP36+ and the outside of the shell. Toward completion of the encapsulation process by capsids with an interior label (AaLS-RR*$^{IN}$), FRET increases as the distance between Top36+ and ATTO-565 decreases, observable by a decrease in donor (TOP36+)


DOI: 10.1021/jacs.5b10588
J. Am. Chem. Soc. 2015, 137, 16121−16132

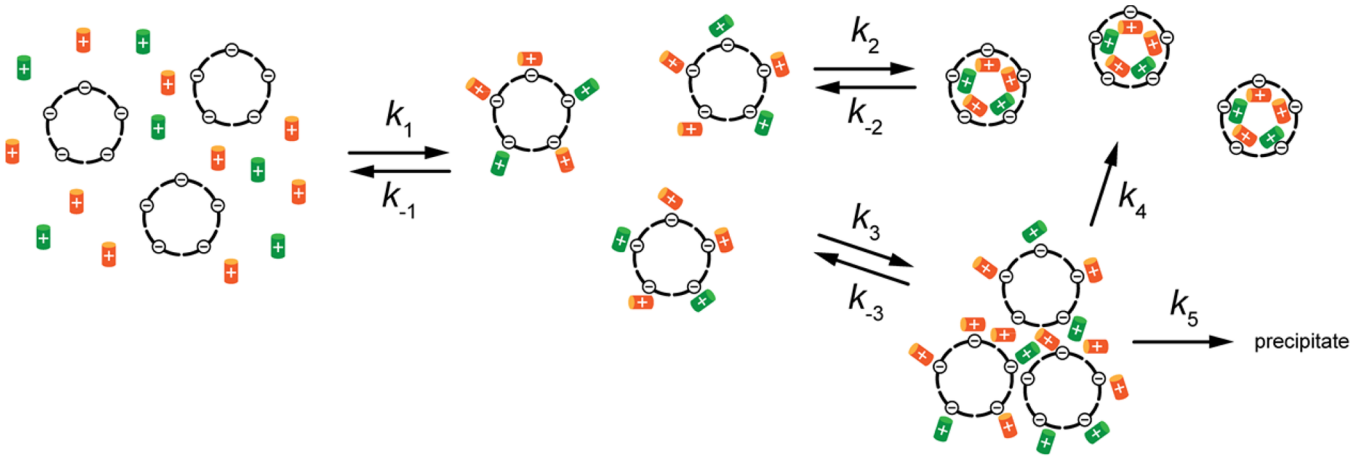


**Figure 10.** Kinetic model for guest encapsulation in AaLS-13 capsids.

fluorescence and an increase in acceptor (ATTO-565) emission (Figure 9B). Complementarily, when TOP36+ migrates from the external capsid surface to the interior, the donor−acceptor distance increases for capsids labeled on the exterior (AaLS-RR*$^{OUT}$), resulting in rising donor (TOP36+) and decreasing acceptor (ATTO-565) emission (Figure 9C). Although mixing AaLS-RR*$^{OUT}$ and TOP36+ ultimately leads to precipitation as apparent from the persistently strong light scattering, the initial fluorescence changes are consistent with migration of TOP36+ from the capsid exterior to the lumen.

**Encapsulation into the AaLS-neg Capsid.** The kinetic experiments with AaLS-13 raise questions about the molecular basis of rapid cargo loading. In order to identify which mutations might confer these unusual properties, we investigated encapsulation by AaLS-neg, the engineered capsid that served as the starting point for directed evolution. Stopped-flow experiments showed that the time-scales for encapsulation of the GFP36+/Top36+ FRET pair are comparable to those for AaLS-13 and AaLS-RR, albeit with a diminished propensity to form intermediate aggregates (Figure S8A). The half-life for cargo exchange between filled AaLS-neg capsids was determined to be 13 ± 7 s, about 3-fold shorter than for AaLS-13 (Figure S8B). These results suggest that the key features enabling capsids to take up globular proteins are already present in AaLS-neg and must therefore be a direct consequence of introducing additional negative charge on the lumenal surface of the capsid.

## DISCUSSION

A protein FRET pair, designed to probe interactions between positively supercharged guest proteins and AaLS-13 capsids, has provided unique insights into the encapsulation of cargo molecules by this engineered protein container. By virtue of the linear dependence of the emission ratio 525/508 nm on capsid occupancy, the GFP36+/ TOP36+ FRET pair provides semiquantitative insight into the composition of filled capsids. However, its true utility is in measuring encapsulation kinetics and the stability of the resulting capsid−guest complexes.

Encapsulation of supercharged guests into assembled AaLS-13 capsid is a robust, reversible process and is unexpectedly fast. Mixing guest and capsid does not immediately afford loaded capsids, but most likely proceeds through an intermediate that exhibits pronounced light scattering. Stopped-flow experiments with TOP36+ and inside or outside labeled AaLS-13 capsids suggest that guest molecules transiently associate with the exterior of the capsids in the intermediate. Based on these observations we propose a multi-step kinetic model for the encapsulation of supercharged guests by AaLS-13 capsids (Figure 10).

Upon encountering the negatively charged shells, the positively charged guests first bind weakly to the exterior capsid surface ($k_1$). The strength of this interaction, modulated by the ionic strength, determines the rate at which the surface bound guest can dissociate and enter the capsid ($k_2$). If this transition is slow, the surface bound guest molecules can act as bridges between capsids and promote aggregation ($k_3$). The resulting colloids cause a transient increase in light scattering. If the interactions are sufficiently weak, the supercharged guest proteins internalize, gradually increasing the negative charge on the capsid's external surface until the individual particles repel each other and the colloids disintegrate ($k_4$). If, however, the Coulombic interactions between guest and capsid surface are too strong, the colloids will continue to grow and eventually precipitate ($k_5$). For example, mixing 20 $\mu$M empty AaLS-13 capsids with 8 $\mu$M GFP36+/TOP36+ leads to precipitation at an ionic strength of 150 mM. A similar mechanism has been proposed by Malyutin and Dragnea to explain intermediate aggregation during nanoparticle-templated assembly of Brome mosaic virus, albeit with opposite roles for capsid protein and guest.[52] In their model, individual capsid proteins act as bridges between nanoparticles, and the dissolution of the colloid is driven by the budding of completed capsids.

Whether mixing empty capsids with cargo results in encapsulation or precipitation depends on the relative rates of the two processes, which can be tuned by varying ionic strength, protein concentration, or charge on the guest molecules. For GFP36+, the previously established standard conditions (50 mM $NaP_i$, 200 mM NaCl, 5 mM EDTA, $I$ = 350 mM)[29] are a good compromise between low salt concentration, which favors capsid−cargo complex formation thermodynamically but leads to unwanted precipitation, and high salt concentration, which diminishes precipitation but also reduces encapsulation yields. For more positively charged oligomeric guests, precipitation can be avoided by increasing ionic strength during encapsulation.[37] The resulting complexes can then be stabilized by subsequently reducing the salt concentration.

By virtue of multivalent interactions between constituent monomers, viral capsids are extremely stable structures.[30] In the absence of an appropriate trigger, dissociation of subunits


DOI: 10.1021/jacs.5b10588
J. Am. Chem. Soc. 2015, 137, 16121−16132

occurs very slowly, if at all.[53] Similarly, the subunit exchange experiments (Figure S6) indicate high kinetic stability of assembled AaLS-13. In this light, rapid internalization of 30 kDa proteins into assembled AaLS-13 capsids is rather surprising and highlights a fundamental difference between this engineered system and typical viral capsids. Applying established principles used to study protein−protein interactions, a bimolecular rate constant of $10^8$ $M^{-1}$ $s^{-1}$ could be determined for guest encapsulation, which approaches the diffusion limit. Since the internalization rate depends on protein concentration, the rate-limiting step must involve the encounter of guests and capsids rather than intrinsic motions of the capsid. Consequently, the protein motions that allow passage of a 30 kDa protein are either surprisingly fast ($\tau$ < 5 ms), or the responsible gateways are already in place.

Rapid encapsulation goes hand in hand with facile release of guest proteins from AaLS-13 capsids. Under standard conditions ($I$ = 350 mM), GFP36+ molecules exchange between capsids with a half-life of <1 min. In contrast, under physiological conditions ($I$ = 160 mM) the half-life increases to 36 h. The latter result implies that on time scales relevant for in vivo applications, the capsid−cargo complex is kinetically stable. This property is desirable for drug delivery applications in which the guests have to remain shielded before reaching their designated destination.

Our experiments demonstrate that the AaLS-13 capsid shell does not pose a physical barrier to molecules as large as GFP, implying that engineering and evolution of AaLS-13 to accommodate positively charged cargo must have had a dramatic effect on its structure, dynamics, or both. Since wild-type AaLS contains pores with a diameter of only 9 Å, the mutations incorporated during the design and subsequent directed evolution of AaLS might have either destabilized the interactions between subunits or endowed the shell with voids large enough to allow transport of sizable proteins across the capsid wall.

Alternative explanations, for example, that the end point of the time course for FRET acceptor emission corresponds to guest molecules bound to the exterior surface of the capsid, can be excluded based on internalization experiments with capsids that were labeled with fluorophores on either the interior or exterior surface. Preorganized voids in the capsid shell could hint at incomplete protein shells or might be an inherent feature of the evolved AaLS-13 capsid. Complete capsids bearing sizable holes are not unprecedented. Bacteriophage P22, for instance, releases a pentamer upon incubation at 70 °C in vitro, yielding a stable capsid with a pore spanning 10 nm.[54]

The notion that the AaLS-13 capsid is highly flexible is supported by the observation that reversion of two mutations, C52R and C127R, afforded capsids that are kinetically labile at low ionic strength (≤350 mM). Hence, subunit interactions in AaLS-13 might be just strong enough to prevent detectable dissociation within a few days, but sufficiently weak to generate transient clefts that allow passage of globular proteins.

Judging from the similar rates of guest encapsulation and cargo exchange for the engineered AaLS-neg and subsequently evolved AaLS-13 variants, the structural features that allow facile entry of protein cargo into assembled capsids were already present in the original design. Electrostatic repulsion between the additional negative charges introduced on the lumenal face of the shell protein may have rendered the capsid subunits less compact and reduced their Gaussian curvature. Adaptation of the subunit structure to the increased local charge density in this way would have facilitated formation of larger polyhedral capsids and while simultaneously the flexibility needed for globular proteins to cross the shell.

Since the ability to encapsulate cargo by assembled capsids is already inherent to AaLS-neg, the improved sequestration achieved by directed evolution presumably reflects the increased charge density in AaLS-13, resulting in tighter binding of positively charged guests.[34] Given the unexpected destabilization of the AaLS-13 capsid upon simple reversion of two residues, it is unlikely that rational design would have identified the optimal compromise required to maximize negative surface charge and maintain capsid stability.

## CONCLUSION

Within the spectrum of capsids that are currently available for biotechnological applications, AaLS-13 is unique in that its loading can be quantitatively controlled in vitro over a broad, physiologically relevant pH range. Formation of host−guest complexes can be precisely regulated by ionic strength and is reversible, rendering AaLS-13 a potentially useful vehicle for targeted delivery of biomacromolecules. Rapid encapsulation strongly suggests that diffusion of small molecules will not be impeded by the AaLS-13 capsid wall. This property should facilitate the design of reaction systems that benefit from high local catalyst concentrations and free diffusion of small molecules.[55] The spectral variants of the encapsulation tag not only allow for simultaneous quantification of different cargo molecules but also permit monitoring of their association under a variety of conditions. In depth understanding of the GFP36+/AaLS-13 encapsulation system together with the spectroscopic tools developed in this work establish a solid foundation for engineering and characterizing multicomponent enzyme nanoreactors.

## EXPERIMENTAL SECTION

**Molecular Cloning.** *Escherichia coli* XL1blue was used as a host for all cloning steps. Plasmids containing confirmed gene sequences were transformed into BL21 gold (DE3) for protein production. Phusion high-fidelity DNA polymerase, restriction enzymes, antarctic phosphatase, and T4 ligase were purchased from New England BioLabs (Ipswich, U.S.A.). Oligonucleotides were synthesized by Microsynth AG (Balgach, Switzerland). Sequences of all modified genes were confirmed by DNA sequencing performed at Microsynth AG (Balgach, Switzerland).

pACYC_His6-TOP(36+) was constructed from pACYC_His6-GFP(36+)[55] by overlap extension PCR using pACYC_fw and pACYC_rv as flanking primers and Top1_fw, Top1_rv, Top2_fw, Top2_rv, Top3_fw, and Top3_rv (Table 1) for iterative introduction of site-directed mutations. The resulting gene product was digested with BamHI and XhoI and subsequently ligated into digested and dephosphorylated pACYC_His6-GFP(36+) to afford pACYC_His6-TOP(36+).

pMG211_AaLS13_A85C was constructed from pMG211_AaLS13[34] by overlap extension PCR using AaLS13_fw and AaLS13_rv as flanking primers and A85C_fw and A85C_rv to introduce mutation A85C. The gene product was digested with NdeI and XhoI and subsequently ligated into digested and dephosphorylated pMG211[56] to afford pMG211_AaLS13_A85C.

pMG211_AaLS13_C52R_C127R was constructed from pMG211_AaLS13 by overlap extension PCR using AaLS13_fw and T7term as flanking primers and C52R_fw, C52R_rv, C127R_fw, and C127R_rv to introduce mutations C52R and C127R. The gene product was digested with NdeI and XhoI and subsequently ligated into digested and dephosphorylated pMG211 to afford pMG211_AaLS13_C52R_C127R. pMG211_AaL-


DOI: 10.1021/jacs.5b10588
J. Am. Chem. Soc. 2015, 137, 16121−16132

Table 1. Oligonucleotides Used for Molecular Biology[a]

| Name | Sequence |
|---|---|
| pACYC_fw | ACTTTTATCTAATCTCGACATCATTAATTCC |
| pACYC_rv | AGCGGTGGCAGCAGCCAACTCAGC |
| T7term | TGCTAGTTATTGCTCAGCGG |
| Top1_fw | TATGGCGTTCAGTGCTTCGCGCGTTACCCTA AACACATG |
| Top1_rv | GAAGCACTGAACGCCATAGCCCAGGGTGGTC ACTAAGG |
| Top2_fw | CGTTACCCTAAACACATGCGCCGTCACGATT TTTTCAAATCAGC |
| Top2_rv | CATGTGTTTAGGGTAACGCGC |
| Top3_fw | CGCAACCACTACCTGAGCTATCGTTCTAAAC TGAGCAAA |
| Top3_rv | GCTCAGGTAGTGGTTGCG |
| AaLS13_fw | AGATATACATATGGAAATCTACGAAGG |
| AaLS13_rv | TGGTGCTCGAGTCGGAGAGACTTGAATAAGT TTGC |
| A85C_fw | ATTGGCGTTCTCATCGAAGGGTGCGAGCCAC ATTTCG |
| A85C_rv | CCCTTCGATGAGAACGCCAATTGC |
| C52R_fw | CGTGAAGAAGACATTACTCTGGTTCGCGTTC CAGGCTCATGGGAAATACC |
| C52R_rv | AACCAGAGTAATGTCTTCTTCACG |
| C127R_fw | CGAATTGGAAGAGGCTATCGAGCGCGCCGGC ACAGAACACGGCAAC |
| C127R_rv | CTCGATAGCCTCTTCCAATTCG |
| R108C_fw | AAACCTATCAGCTTCGGTGATATTAC |
| R108C_rv | GTAATATCACCGAAGCTGATAGGTTTACATA GTTCTAATGAAAGGTTCGCG |

[a]Mutated codons are underlined; restriction sites are surrounded by a box.

S13_C52R_A85C_C127R was constructed analogously using pMG211_AaLS13_A85C as template.

pMG211_AaLS13_C52R_R108C_C127R was constructed from pMG211_AaLS13_C52R_C127R using AaLS_fw and AaLS_rv as flanking primers and R108C_fw and R108C_rv to introduce mutation R108C. The gene product was digested with NdeI and XhoI and subsequently ligated into digested and dephosphorylated pMG211 to afford pMG211_AaLS13_C52R_C127R_R108C.

**Protein Production and Purification.** *GFP36+ and TOP36+.* A dense overnight culture of BL21 gold (DE3) carrying either plasmid pACYC_His6-GFP36+ or pACYC_His6-TOP36+ was used to inoculate 400 mL of LB medium supplemented with 36 μg/mL chloramphenicol and incubated at 37 °C and 230 rpm until $OD_{600}$ reached 0.6−0.7. Following addition of 100 μM IPTG, the temperature was reduced to 25 °C, and incubation continued for 20 h. Cultures were centrifuged at 4 °C and 4000 *g* for 20 min, and the resulting cell pellet stored at −20 °C. The cell pellet was thawed and suspended in lysis buffer (50 mM $NaP_i$, 2 M NaCl, pH 7.4) supplemented with 1 mg/mL lysozyme, protease inhibitor cocktail, and a spatula tip of both DNase I and RNase A. Following incubation at room temperature for 1 h, cells were lysed by sonication, and the insoluble fraction removed by centrifugation at 4 °C and 14,000 *g* for 30 min. The clear lysate was loaded on 4 mL of Ni-NTA agarose resin equilibrated with lysis buffer. Following washing with lysis buffer and lysis buffer containing 20 mM imidazole, the protein was eluted with lysis buffer containing 250 mM imidazole. Protein-containing fractions were concentrated, and the buffer changed to 50 mM Tris-HCl, 500 mM NaCl, pH 7.4 using a centrifugal ultrafiltration unit (10 kDa MWCO, Amicon Ultra, Merck Millipore). The concentrated protein was further purified by ion exchange chromatography using a Mono S HR 10/10 column (GE Healthcare Life Sciences, U.K.) that had been equilibrated with 50 mM Tris-HCl, 500 mM NaCl, pH 7.4 at 4 °C using a linear gradient to 50 mM Tris-HCl, 1.5 M NaCl, pH 7.4. Protein-containing fractions were combined, concentrated, exchanged to 50 mM $NaP_i$, 600 mM NaCl, 5 mM EDTA, pH 8.0 and stored at 4 °C.

*AaLS-13 and Variants Thereof.* A dense overnight culture of BL21 gold (DE3) carrying plasmid pMG211_AaLS13 or a variant thereof was used to inoculate 400 mL of LB-medium supplemented with 150 μg/mL ampicillin and incubated at 37 °C and 230 rpm until $OD_{600}$ reached 0.6−0.7. Following addition of 100 μM IPTG, the temperature was reduced to 30 °C, and incubation continued for 20 h. Cultures were centrifuged at 4 °C and 4000 *g* for 20 min, and the resulting cell pellet stored at −20 °C. The cell pellet was thawed and suspended in lysis buffer (50 mM $NaP_i$, 300 mM NaCl, pH 8.0) supplemented with 1 mg/mL lysozyme, protease inhibitor cocktail, and a spatula tip of both DNase I and RNase A. Following incubation at room temperature for 1 h, cells were lysed by sonication, and the insoluble fraction removed by centrifugation at 25 °C and 14,000 *g* for 30 min. The cleared lysate was loaded on 4 mL of Ni-NTA agarose resin equilibrated with lysis buffer. Following washing with lysis buffer containing 20 or 40 mM imidazole, the protein was eluted with lysis buffer containing 500 mM imidazole. Immediately after elution, 5 mM EDTA was added to the protein solution.

In order to obtain assembled capsids, buffer was changed to 50 mM $NaP_i$, 600 mM NaCl, 5 mM EDTA, pH 8.0 using a centrifugal ultrafiltration unit (30 kDa MWCO, Amicon Ultra, Merck Millipore). The protein was incubated at a concentration of 1−2 mM for 5−7 days at room temperature before separating capsids from fragments (mostly pentamers) by size-exclusion chromatography using a HiPrep 16/60 Sephacryl S-400 column (GE Healthcare Life Sciences, U.K.). To obtain the capsid fragments, buffer was changed to 50 mM $NaP_i$, 100 mM NaCl, 5 mM EDTA, and the quaternary states were separated without delay. In the case of AaLS-13 variants containing an additional cysteine residue intended for chemical modification, 5 mM TCEP was added. Purified protein was stored in either 50 mM $NaP_i$, 100 mM NaCl, 5 mM EDTA, pH 8.0 (fragments) or 50 mM $NaP_i$, 200 mM NaCl, 5 mM EDTA, pH 8.0 (assembled capsids) at room temperature.

*Covalent Labeling of AaLS-13 Variants.* Reagents for covalent labeling of AaLS-13 variants with fluorophores were selected such that modification would occur selectively at cysteine residues introduced by site-directed mutagenesis. In order to promote labeling of the strongly negatively charged protein, positively charged ATTO-495-maleimide and neutral ATTO-565-maleimide (ATTO-Tec, Germany) were chosen. Between 0.2 and 0.3 equiv of reactive dye were added to a 50−300 μM solution of AaLS-13 A85C or AaLS-13 C52R/A85C/C127R in 50 mM $NaP_i$, 200 mM NaCl, 5 mM EDTA, pH 8.0, and the resulting mixture incubated at room temperature in the dark for 1 h before quenching the reaction by addition of 1 mM β-mercaptoethanol. Small molecules were removed using a PD-10 column (GE Healthcare Life Sciences, U.K.). Quarternary states were subsequently separated by size-exclusion chromatography using a HiPrep 16/60 Sephacryl S-400 column (GE Healthcare Life Sciences, U.K.). The extent of labeling was calculated from UV−vis spectra of the labeled proteins using $\varepsilon_{565\ nm}$(ATTO-565) = 120,000 $M^{-1}$ $cm^{-1}$, $\varepsilon_{280\ nm}$(ATTO-565) = 19,200 $M^{-1}$ $cm^{-1}$, $\varepsilon_{495\ nm}$(ATTO-495) = 80,000 $M^{-1}$ $cm^{-1}$, $\varepsilon_{280\ nm}$(ATTO-495) = 31,200 $M^{-1}$ $cm^{-1}$, and $\varepsilon_{280\ nm}$(AaLS) = 13,980 $M^{-1}$ $cm^{-1}$. Typically 10−16% of the monomers were labeled.

Labeling AaLS-13 C52R/R108C/C127R bearing an exposed thiol on the exterior surface with ATTO-565-maleimide under identical conditions resulted in a significantly lower labeling ratio (4%). In order to improve labeling, the reaction was carried out under modified conditions in 50 mM $NaP_i$, 1 M NaCl, 5 mM EDTA, pH 8.0, using 2.0 equiv of reagent for an extended incubation time of 12 h, yielding 27−55% labeled monomers (AaLS-RR*$^{OUT}$).

**Concentration Determination.** Protein concentrations were determined from UV−vis absorption spectra between 250 and 800



DOI: 10.1021/jacs.5b10588
J. Am. Chem. Soc. 2015, 137, 16121−16132

nm recorded on a Lambda 20 or Lambda 35 spectrophotometer (PerkinElmer, U.S.A.). For samples containing capsids, the contribution of particle-induced light scattering was taken into account by fitting eq 1 to regions of the spectra devoid of absorption bands (350–600 nm for empty, unlabeled capsids, 550–800 nm for capsid–cargo complexes and 600–800 nm for chemically labeled capsids) using ale - UV–vis-IR Spectral Software 2.0 (FluorTools, www.fluortools.com).

$$A_{\text{scatter}}(\lambda) = A_0 + \log \frac{1}{1 - c\cdot\lambda^4} \quad (1)$$

By virtue of their distinctive absorption spectra, the concentrations of the individual components in mixtures of AaLS-13, GFP36+ and TOP36+ can be determined by solving a system of linear equations accounting for the individual contributions of each component to the total absorption at three different wavelengths. The extinction coefficient for AaLS-13 was calculated with $\varepsilon_{280\text{ nm}}$(AaLS-13) = 13,980 $M^{-1}$ $cm^{-1}$, using ProtPram (http://expasy.org/tools/protparam.html). Extinction coefficients for GFP36+ are $\varepsilon_{280\text{ nm}}$ = 17,420 $M^{-1}$ $cm^{-1}$, $\varepsilon_{488\text{ nm}}$ = 36,600 $M^{-1}$ $cm^{-1}$, and $\varepsilon_{513\text{ nm}}$ = 6,010 $M^{-1}$ $cm^{-1}$.[55] The extinction coefficients for TOP36+ were determined to be $\varepsilon_{280\text{ nm}}$ = 20,610 $M^{-1}$ $cm^{-1}$, $\varepsilon_{488\text{ nm}}$ = 28,610 $M^{-1}$ $cm^{-1}$, and $\varepsilon_{513\text{ nm}}$ = 69,800 $M^{-1}$ $cm^{-1}$ as previously described.[55]

**Fluorescence Measurements.** Fluorescence spectra were recorded on a QuantaMaster 7 (Photon Technology International, U.S.A.) at 25 °C.

*Quantum Yields.* Quantum yields were measured at 25 °C on a Fluorolog 3 spectrofluorimeter (Horiba, Japan) using excitation and emission correction. Quantum yield values for GFP36+ and TOP36+ were determined by the reference method with fluorescein (Fluka, Switzerland) in 0.1 M NaOH and rhodamine 6G (Fluka, Switzerland) in EtOH as reference standards with reported quantum yields of 0.91 ± 0.05 and 0.94, respectively.[57] Diluted solutions of the fluorescent proteins were prepared in either 50 mM $NaP_i$, pH 8.0 or 50 mM Tris-$H_2SO_4$, pH 8.0 so that the optical density at the excitation wavelength was below 0.05 au. No difference in quantum yield was observed between these two buffers. Use of NaCl was avoided as halides are known to quench the fluorescence of YFP variants.[41] Different dilutions of fluorescein and GFP36+ were excited between 410 and 450 nm, and the area of the emission peak (460–660 nm) was plotted as a function of the optical density at the excitation wavelength. Similar plots were prepared for TOP36+ (excitation 420–460 nm; emission 470–670 nm) and rhodamine 6G (excitation 450–490 nm; emission 500–700 nm). Quantum yields of GFP36+ and TOP36+ were calculated by relating the respective slopes to fluorescein. Comparison between fluorescein and rhodamine 6G was used to validate the procedure.

*pH and Ionic Strength Dependence.* Empty AaLS-13 capsids were mixed with a 1:4 mixture of GFP36+/TOP36+ at an ionic strength of 350 mM, pH 8.0, 25 °C and purified by size-exclusion chromatography under the same conditions. Buffers were prepared using MES (pH 6–6.5), HEPES (pH 7–8), CHES/HEPES (pH 8.5), CHES (8.5–9.5), CHES/CAPS (pH 10), or CAPS (pH 10.5–11), and pH was adjusted by addition of NaOH. Concentrated capsid–guest complexes or a mixture of guests were diluted into a solution containing 25 mM buffer and 200 mM NaCl.

A solution containing purified capsid–cargo complex in 50 mM $NaP_i$, 5 mM EDTA, pH 8.0 was titrated with 50 mM $NaP_i$, 4 M NaCl, 5 mM EDTA, pH 8.0 containing an identical concentration of the same complex in order to keep concentrations of proteinaceous solutes constant when determining the effect of ionic strength on the FRET efficiency between encapsulated GFP36+ and TOP36+.

**Kinetic Measurements.** *Guest Exchange between Capsids.* Buffers of different ionic strength were prepared by mixing 50 mM $NaP_i$, 5 mM EDTA, pH 8.0 and 50 mM $NaP_i$, 1 M NaCl, 5 mM EDTA, pH 8.0 in appropriate ratios. After mixing AaLS-13 containing GFP36+ and AaLS-13 containing Top36+ in a 1:4 ratio at 25 °C, the time course of fluorescence emission was followed at 508 or 525 nm upon irradiation at 400 nm. The rate constant for guest exchange $k$ was determined by fitting the trace at 525 nm to eq 2 in which the linear term accounts for time-dependent photobleaching of the chromophores.

$$F(t) = F_0 + \Delta F\cdot e^{-kt} + G\cdot t \quad (2)$$

*Stopped Flow Measurements.* Guest encapsulation in AaLS-13 variants was observed by following the change in fluorescence emission upon mixing supercharged protein guests with empty capsids in a SX18-MV stopped-flow spectrometer (Applied Photophysics, U.K.) equilibrated with a water bath at 25 °C. For each transient, 1000 data points were recorded using a logarithmic time base over 10 s, and 8–10 transients were averaged for each experiment. Due to the availability of less material, only three transients were averaged for experiments involving chemically labeled AaLS-13 variants.

For encapsulation experiments with mixtures of GFP36+ and TOP36+, the mixing cell was irradiated at 400 nm, and fluorescence emission detected at a 90° angle. GFP36+ emission was selectively detected using a band-pass filter with center wavelength at 500 nm and a full width at half-maximum (fwhm) of 10 nm (Laser Components GmbH, Germany); a long pass filter with an edge at 515 nm (Applied Photophysics, U.K.) was used for TOP36+ emission. For encapsulating TOP36+ in AaLS-13 variants labeled with ATTO-565, irradiation occurred at 450 nm, and TOP36+ emission was selectively detected using a band-pass filter with a center wavelength at 525 nm and fwhm of 25 nm (Edmund Optics Inc., U.S.A.), while a long pass filter with an edge at 570 nm (Applied Photophysics, U.K.) was used for ATTO-565 emission. Light scattering was detected by either absorption at 400 nm or irradiation between 600 and 650 nm combined with a photomultiplier positioned at a 90° angle. Both methods were used in conjunction to confirm that signal changes arose from light scattering by colloidal particles and not changes in the light-transmissive or fluorescent properties of the chromophores. The slit widths of the monochromator used to select the wavelength for irradiation and the photomultiplier voltage were adjusted for each experiment and signal channel to optimize the signal-to-noise ratio. Consequently, the amplitudes of transients cannot be compared between experiments, unless explicitly stated.

At low protein concentrations for which intermediate aggregation was not observed, second-order kinetics were assumed for the association between guest proteins and binding sites within the capsid (a binding site spans approximately five capsid monomers). If the starting concentrations of both reactants are set equal, the time dependence of the fluorescence emission can be described by eq 3.

$$F(t) = F_0 + \Delta F\cdot\frac{c_0^2 k_1 t}{1 + c_0 k_1 t} \quad (3)$$

Even if the initial concentrations of the two components are not exactly identical, this equation serves as a good approximation in which $c_0$ is calculated as the average of guest and binding site concentration.[58] For different starting concentrations, $c_0$, eq 3 is fitted to the progress curve of TOP36+ emission to determine $c_0k_1$. Linear regression of $c_0k_1$ against $c_0$ yields the bimolecular rate constant for association $k_1$.

**Calculation of the Electrostatic Surface Potential.** The crystal structure of wild-type AaLS, PDB code 1HQK,[35] was relaxed under symmetry constraints[59] using Rosetta 3.4[60] before introducing mutations for AaLS-13 by *fixbb*, followed by another round of relaxation. The resulting structure was used as input to calculate the surface electric potential at $I$ = 150 mM, pH 8.0 using the adaptive Poisson–Boltzmann solver.[49]

## ■ ASSOCIATED CONTENT

### Supporting Information

The Supporting Information is available free of charge on the ACS Publications website at DOI: 10.1021/jacs.5b10588.

Additional fluorescence data, chromatograms, and EM pictures (PDF)



DOI: 10.1021/jacs.5b10588
J. Am. Chem. Soc. 2015, 137, 16121–16132

## AUTHOR INFORMATION


### Corresponding Author

*hilvert@org.chem.ethz.ch


### Notes

The authors declare no competing financial interest.

## ACKNOWLEDGMENTS

We are indebted to Eva van Rooden (Erasmus scholar) for cloning, expressing, and purifying TOP36+ and are grateful to Ben Schuler and Andrea Holla at the Department of Biochemistry, University of Zurich for help determining quantum yields and Peter Tittmann at the Scientific Center for Optical and Electron Microscopy (ScopeM), ETH Zurich for assistance with electron microscopy experiments. This work was generously supported by the ETH Zurich and the European Research Council (Advanced ERC grant ERC-dG-2012-321295 to D.H.). R.Z. is grateful for a scholarship from the Stipendienfonds der Schweizerischen Chemischen Industrie (SSCI).

## REFERENCES


(1) van der Schoot, P.; Zandi, R. *Phys. Biol.* **2007**, *4*, 296−304.
(2) Zlotnick, A.; Fane, B. A. In *Structural Virology*; Royal Society of Chemistry: Cambridge, 2011; pp 180−202.
(3) Šiber, A.; Božič, A. L.; Podgornik, R. *Phys. Chem. Chem. Phys.* **2012**, *14*, 3746−3765.
(4) Perlmutter, J. D.; Hagan, M. F. *Annu. Rev. Phys. Chem.* **2015**, *66*, 217−239.
(5) Flenniken, M. L.; Uchida, M.; Liepold, L. O.; Kang, S.; Young, M. J.; Douglas, T. *Curr. Top. Microbiol. Immunol.* **2009**, *327*, 71−93.
(6) Steinmetz, N. F.; Lin, T.; Lomonossoff, G. P.; Johnson, J. E. *Curr. Top. Microbiol. Immunol.* **2009**, *327*, 23−58.
(7) Manchester, M.; Steinmetz, N. F. *Viral Nanoparticles: Tools for Materials Science & Biomedicine*; Pan Stanford Publishing: Singapore, 2011.
(8) Tan, M.; Jiang, X. *Curr. Opin. Virol.* **2014**, *6*, 24−33.
(9) Lee, S. Y.; Lim, J. S.; Harris, M. T. *Biotechnol. Bioeng.* **2012**, *109*, 16−30.
(10) Ma, Y.; Nolte, R. J. M.; Cornelissen, J. J. L. M. *Adv. Drug Delivery Rev.* **2012**, *64*, 811−825.
(11) Shukla, S.; Steinmetz, N. F. *WIREs Nanomed. Nanobiotechnol.* **2015**, *7*, 708−721.
(12) Bode, S. A.; Minten, I. J.; Nolte, R. J. M.; Cornelissen, J. J. L. M. *Nanoscale* **2011**, *3*, 2376−2389.
(13) Cardinale, D.; Carette, N.; Michon, T. *Trends Biotechnol.* **2012**, *30*, 369−376.
(14) Yeates, T. O.; Kerfeld, C. A.; Heinhorst, S.; Cannon, G. C.; Shively, J. M. *Nat. Rev. Microbiol.* **2008**, *6*, 681−691.
(15) Tanaka, S.; Kerfeld, C. A.; Sawaya, M. R.; Cai, F.; Heinhorst, S.; Cannon, G. C.; Yeates, T. O. *Science* **2008**, *319*, 1083−1086.
(16) Wheatley, N. M.; Gidaniyan, S. D.; Liu, Y.; Cascio, D.; Yeates, T. O. *Protein Sci.* **2013**, *22*, 660−665.
(17) Yeates, T. O.; Thompson, M. C.; Bobik, T. A. *Curr. Opin. Struct. Biol.* **2011**, *21*, 223−231.
(18) Klein, M. G.; Zwart, P.; Bagby, S. C.; Cai, F.; Chisholm, S. W.; Heinhorst, S.; Cannon, G. C.; Kerfeld, C. A. *J. Mol. Biol.* **2009**, *392*, 319−333.
(19) Kim, E. Y.; Tullman-Ercek, D. *Biotechnol. J.* **2014**, *9*, 348−354.
(20) Chessher, A.; Breitling, R.; Takano, E. *ACS Biomater. Sci. Eng.* **2015**, *1*, 345−351.
(21) Kim, E. Y.; Tullman-Ercek, D. *Curr. Opin. Biotechnol.* **2013**, *24*, 627−632.
(22) Patterson, D. P.; Schwarz, B.; Waters, R. S.; Gedeon, T.; Douglas, T. *ACS Chem. Biol.* **2014**, *9*, 359−365.
(23) O'Neil, A.; Reichhardt, C.; Johnson, B.; Prevelige, P. E.; Douglas, T. *Angew. Chem., Int. Ed.* **2011**, *50*, 7425−7428.
(24) Minten, I. J.; Hendriks, L. J. A.; Nolte, R. J. M.; Cornelissen, J. J. L. M. *J. Am. Chem. Soc.* **2009**, *131*, 17771−17773.
(25) Fiedler, J. D.; Brown, S. D.; Lau, J. L.; Finn, M. G. *Angew. Chem., Int. Ed.* **2010**, *49*, 9648−9651.
(26) Rurup, W. F.; Snijder, J.; Koay, M. S. T.; Heck, A. J. R.; Cornelissen, J. J. L. M. *J. Am. Chem. Soc.* **2014**, *136*, 3828−3832.
(27) Seebeck, F. P.; Woycechowsky, K. J.; Zhuang, W.; Rabe, J. P.; Hilvert, D. *J. Am. Chem. Soc.* **2006**, *128*, 4516−4517.
(28) Brasch, M.; de la Escosura, A.; Ma, Y.; Uetrecht, C.; Heck, A. J. R.; Torres, T.; Cornelissen, J. J. L. M. *J. Am. Chem. Soc.* **2011**, *133*, 6878−6881.
(29) Wörsdörfer, B.; Pianowski, Z.; Hilvert, D. *J. Am. Chem. Soc.* **2012**, *134*, 909−911.
(30) Katen, S.; Zlotnick, A. *Methods Enzymol.* **2009**, *455*, 395.
(31) Singh, S.; Zlotnick, A. *J. Biol. Chem.* **2003**, *278*, 18249−18255.
(32) Bacher, A.; Ludwig, H. C.; Schnepple, H.; Ben-Shaul, Y. *J. Mol. Biol.* **1986**, *187*, 75−86.
(33) Ladenstein, R.; Fischer, M.; Bacher, A. *FEBS J.* **2013**, *280*, 2537−2563.
(34) Wörsdörfer, B.; Woycechowsky, K. J.; Hilvert, D. *Science* **2011**, *331*, 589−592.
(35) Zhang, X.; Meining, W.; Fischer, M.; Bacher, A.; Ladenstein, R. *J. Mol. Biol.* **2001**, *306*, 1099−1114.
(36) Lawrence, M. S.; Phillips, K. J.; Liu, D. R. *J. Am. Chem. Soc.* **2007**, *129*, 10110−10112.
(37) Beck, T.; Tetter, S.; Künzle, M.; Hilvert, D. *Angew. Chem., Int. Ed.* **2015**, *54*, 937−940.
(38) O'Neil, A.; Prevelige, P. E.; Basu, G.; Douglas, T. *Biomacromolecules* **2012**, *13*, 3902−3907.
(39) Rurup, W. F.; Verbij, F.; Koay, M. S. T.; Blum, C.; Subramaniam, V.; Cornelissen, J. J. L. M. *Biomacromolecules* **2014**, *15*, 558−563.
(40) Cubitt, A. B.; Woollenweber, L. A.; Heim, R. *Methods Cell Biol.* **1998**, *58*, 19−30.
(41) Wachter, R. M.; Remington, S. J. *Curr. Biol.* **1999**, *9*, R628−R629.
(42) Patterson, G. H.; Piston, D. W.; Barisas, B. G. *Anal. Biochem.* **2000**, *284*, 438−440.
(43) Fábián, Á. I.; Rente, T.; SzölloSi, J.; Matyus, L.; Jenei, A. *ChemPhysChem* **2010**, *11*, 3713−3721.
(44) Zheng, J. In *Handbook of Modern Biophysics*; Jue, T., Ed.; Humana Press: Totowa, NJ, 2010; Vol. 3, pp 119−136.
(45) Bai, X.; McMullan, G.; Scheres, S. H. *Trends Biochem. Sci.* **2015**, *40*, 49−57.
(46) Snijder, J.; Van De Waterbeemd, M.; Damoc, E.; Denisov, E.; Grinfeld, D.; Bennett, A.; Agbandje-Mckenna, M.; Makarov, A.; Heck, A. J. R. *J. Am. Chem. Soc.* **2014**, *136*, 7295−7299.
(47) Israelachvili, J. N. In *Intermolecular and Surface Forces*, 3rd ed.; Academic Press: Waltham, MA, 2011; pp 291−340.
(48) Kegel, W. K.; van der Schoot, P. *Biophys. J.* **2004**, *86*, 3905−3913.
(49) Baker, N. A.; Sept, D.; Joseph, S.; Holst, M. J.; McCammon, J. A. *Proc. Natl. Acad. Sci. U. S. A.* **2001**, *98*, 10037−10041.
(50) Griesbeck, O.; Baird, G. S.; Campbell, R. E.; Zacharias, D. A.; Tsien, R. Y. *J. Biol. Chem.* **2001**, *276*, 29188−29194.
(51) Min, J.; Kim, S.; Lee, J.; Kang, S. *RSC Adv.* **2014**, *4*, 48596−48600.
(52) Malyutin, A. G.; Dragnea, B. *J. Phys. Chem. B* **2013**, *117*, 10730−10736.
(53) Uetrecht, C.; Watts, N. R.; Stahl, S. J.; Wingfield, P. T.; Steven, A. C.; Heck, A. J. R. *Phys. Chem. Chem. Phys.* **2010**, *12*, 13368−13371.
(54) Teschke, C. M.; McGough, A.; Thuman-Commike, P. A. *Biophys. J.* **2003**, *84*, 2585−2592.
(55) Azuma, Y.; Zschoche, R.; Tinzl, M.; Hilvert, D. *Angew. Chem., Int. Ed.*, DOI: 10.1002/anie.201508414, in press.
(56) Sasso, S.; Ramakrishnan, C.; Gamper, M.; Hilvert, D.; Kast, P. *FEBS J.* **2005**, *272*, 375−389.
(57) Brouwer, A. M. *Pure Appl. Chem.* **2011**, *83*, 2213−2228.




DOI: 10.1021/jacs.5b10588
*J. Am. Chem. Soc.* 2015, 137, 16121−16132

(58) Fersht, A. *Structure and Mechanism in Protein Science: A Guide to Enzyme Catalysis and Protein Folding*; W. H. Freeman and Co.: New York, 1999.
(59) DiMaio, F.; Leaver-Fay, A.; Bradley, P.; Baker, D.; André, I. *PLoS One* **2011**, *6*, e20450.
(60) Leaver-Fay, A.; Tyka, M.; Lewis, S. M.; Lange, O. F.; Thompson, J.; Jacak, R.; Kaufman, K. W.; Renfrew, P. D.; Smith, C. A.; Sheffler, W.; Davis, I. W.; Cooper, S.; Treuille, A.; Mandell, D. J.; Richter, F.; Ban, Y.-E. A.; Fleishman, S. J.; Corn, J. E.; Kim, D. E.; Lyskov, S.; Berrondo, M.; Mentzer, S.; Popović, Z.; Havranek, J. J.; Karanicolas, J.; Das, R.; Meiler, J.; Kortemme, T.; Gray, J. J.; Kuhlman, B.; Baker, D.; Bradley, P. *Methods Enzymol.* **2011**, *487*, 545−574.


DOI: 10.1021/jacs.5b10588
*J. Am. Chem. Soc.* 2015, 137, 16121−16132